NANO FUTURES

PAPER

Enhancing photodetection of WSe_2 phototransistors by reducing charge scattering with hBN passivation

Sunggyu Ryoo[1,5], **Taehee Kim**[2,5], **Jongeun Yoo**[1], **Seongmin Ko**[1], **Kyungjune Cho**[3,4,*] and **Takhee Lee**[1,*]

[1] Department of Physics and Astronomy, and Institute of Applied Physics, Seoul National University, Seoul 08826, Republic of Korea
[2] Korean Minjok Leadership Academy, Gangwon 25268, Republic of Korea
[3] Convergence Research Center for Solutions to Electromagnetic Interference in Future-mobility, Korea Institute of Science and Technology, Seoul 02792, Republic of Korea
[4] Electronic and Hybrid Materials Research Center, Korea Institute of Science and Technology, Seoul 02792, Republic of Korea
[5] These authors contributed equally to this work.
[*] Authors to whom any correspondence should be addressed.

E-mail: kcho@kist.re.kr and tlee@snu.ac.kr

Keywords: dielectric disorder, phototransistor, low-frequency noise, transition metal dichalcogenide

Supplementary material for this article is available online

RECEIVED
16 July 2025

ACCEPTED FOR PUBLICATION
18 July 2025

PUBLISHED
29 July 2025

Abstract

Two-dimensional (2D) semiconductors like tungsten diselenide (WSe_2) have significant potential for next-generation phototransistors because of their broad detection range and strong light-matter interaction. However, dielectric disorder at the interface with conventional silicon dioxide (SiO_2) substrates hampers the device performance by introducing surface charge traps and oxygen dangling bonds, which degrade carrier transport and increase low-frequency noise (LFN). Here, we show that simply incorporating a hexagonal boron nitride (hBN) passivation layer between WSe_2 and SiO_2 effectively reduces interfacial disorder by creating a clean van der Waals interface through optoelectrical and LFN analysis. The WSe_2/hBN phototransistors demonstrate a 100-fold decrease in LFN, a 100-fold increase in responsivity, and a 10-fold improvement in specific detectivity compared to WSe_2 devices without an hBN layer. This enhancement in device performance is ascribed to shielding Coulomb scattering and maintaining the intrinsic transport properties of WSe_2. Our findings underscore the importance of passivating the channel scattering sources of 2D-based phototransistors in enhancing photodetection performance.

1. Introduction

Two-dimensional (2D) semiconductors, like transition metal dichalcogenides (TMDs), are considered next-generation semiconductors due to their potential for overcoming the bulk materials' thickness limits [1–4]. Specifically, TMDs are promising phototransistor materials due to their strong light-matter interaction, wide detection range, and interesting photonic phenomena [5–13]. However, a major drawback of low-dimensional materials, including TMDs, is their susceptibility to dielectric disorder, which dominates the optical and electronic properties of devices compared to bulk materials [14, 15].

The major feature of the dielectric disorder is the Coulomb scattering effect during carrier transport, originating from a variety of impurities of the dielectric and the interface [1, 7, 16]. Coulomb scattering leads to a decline in device mobility, a reduction in the current level, and an increase in the device's low-frequency noise (LFN) [15–18]. Since reduced current and increased LFN degrade the performance of phototransistors, minimizing Coulomb scattering induced by the dielectric is essential [19, 20]. Changing the dielectric to high-k or ferroelectric materials is a good solution to address these issues, due to their shielding effect against the scattering sources [21–24]. However, high-k dielectric can induce serious surface optical phonons, and ferroelectric dielectric can induce unintended electrostatic doping due to polarization effects [25–27]. Since then, dielectrics with almost zero dangling bonds, like hexagonal boron nitride (hBN), have been employed to mitigate the dielectric disorder [28, 29]. Utilizing hBN is a great solution to dielectric disorder, owing to its clean interface with TMDs and the absence of phonon-related penalties.

In our study, we reduced LFN and preserved the intrinsic carrier transport properties for enhancing the photodetection performance of tungsten diselenide (WSe_2) phototransistors by separating WSe_2 and amorphous silicon dioxide (SiO_2) using hBN. The hBN, a well-known material that acts as a passivation layer, effectively suppressed the dielectric disorder by forming a van der Waals gap with the WSe_2 channel. The hBN layer improved the overall photodetection performance of WSe_2/hBN devices by a 100-fold reduction in LFN, a 100-fold improvement in responsivity, and a 10-fold enhancement in specific detectivity compared to WSe_2 devices without hBN. This study highlights that passivating the scattering sites of the channel-dielectric interface of the 2D-based phototransistors using dangling-bond-free materials is effective in enhancing photodetection performance.

2. Experiment

The hBN and WSe_2 flakes (both purchased from HQ Graphene) were mechanically exfoliated from bulk crystals and transferred onto a 270 nm SiO_2/p++ Si substrate. Using an optical microscope and an atomic force microscopy (AFM) system (NX-10, Park Systems), thick hBN and few-layer WSe_2 flakes were selected. For WSe_2/hBN heterostructures, a selected few-layer WSe_2 flakes were layered on top of the hBN flakes using the stamping technique with a manipulator (AP-4200, Unitek). Here, we used propylene carbonate-coated polydimethylsiloxane stamps for improved adhesion with WSe_2. After preparing the channel layers, we spin-coated the flakes with methyl methacrylate and poly methyl methacrylate to create a double-electroresist layer. Source and drain electrodes were patterned using an electron-beam lithography system (JSM-6510, JEOL), and a 40 nm layer of gold was deposited using an electron-beam evaporator (KVE2004, Korea Vacuum Tech). Completed phototransistors were heated at 200 °C for 2 h in an argon environment via a rapid thermal annealing system (KVR-4000, Korea Vacuum Tech) to enhance their electrical properties. More details on device fabrication can be found in figure S1 of the supplementary information.

The electrical characteristics and LFN analysis of the WSe_2/hBN devices were measured with a probe station (M6VC, MSTECH) and a semiconductor parameter analyzer (Keithley 4200). The photodetection performance was measured under constant laser illumination at a wavelength of 532 nm with varying powers. The laser beam illuminated the phototransistors globally, with a size specified at a few millimeters in diameter. All characterizations were conducted at room temperature and in a vacuum to eliminate the effects of extraneous variables such as humidity or other gases present in the air. Also, all devices were stored in a vacuum desiccator.

3. Results and discussion

The WSe_2/hBN devices were observed via optical characterization. The optical image of a WSe_2/hBN device can be seen in figure 1(a). The thickness of hBN and WSe_2 flakes was measured using an AFM (figure 1(b)). We employed thick hBN over 30 nm and a few-layer WSe_2 near 15 nm (supplementary figure S2). Figures 1(c) and (d) are the photoluminescence (PL) and the Raman mapping images of the WSe_2/hBN device, illustrating that the WSe_2/hBN heterostructure was successfully constructed. For PL measurements, the hBN displayed deep ultraviolet emission, which fell outside the measurement range, whereas the WSe_2 flake exhibited a prominent A peak (∼780 nm) [30, 31]. Additionally, the E_{2g} peak (∼1365 cm^{-1}) of the hBN and the $E^1{}_{2g}$ peak (∼248 cm^{-1}) of the WSe_2 were clearly shown in Raman spectroscopy [30, 32]. Figure 1(e) presents a schematic of the phototransistor experimental setup. A 532 nm laser was used and modulated with a chopper. The device current was measured using a semiconductor parameter analyzer while applying gate and drain voltages. Subsequently, the optoelectrical properties of the device, including LFN analysis and photodetection performance calculations, were evaluated.

Figure 2(a) shows the transfer characteristics (drain current versus gate voltage, $I_D - V_G$) of representative WSe_2 and WSe_2/hBN devices. Both the WSe_2 and WSe_2/hBN devices exhibited ambipolar behaviors; however, the n-type properties of the WSe_2/hBN devices were prominent compared to the WSe_2 devices. The gate leakage current was sufficiently small to be considered negligible in further analysis (supplementary figure S3). Also, the output characteristics (drain current versus drain voltage, $I_D - V_D$) of the WSe_2 and WSe_2/hBN devices showed that the WSe_2/hBN device's drain current was significantly higher than that of the WSe_2 device, as shown in figure 2(b). This trend was consistently observed in other devices as well (supplementary figure S4). These indicate that the insertion of hBN layer between the WSe_2 flake and SiO_2 substrate can enhance the electron transport properties of a transistor. In addition to modifying electrical properties, hBN also played a critical role in determining the LFN characteristics of the device. Figure 2(c) shows the device's normalized noise (normalized power spectral density with drain current). The LFN of the WSe_2-based devices exhibited a $1/f$ noise-like characteristic since the $1/f$ noise is the primary noise source of 2D TMDs [18, 33, 34]. For more details about the LFN analysis, see figure S5 of the

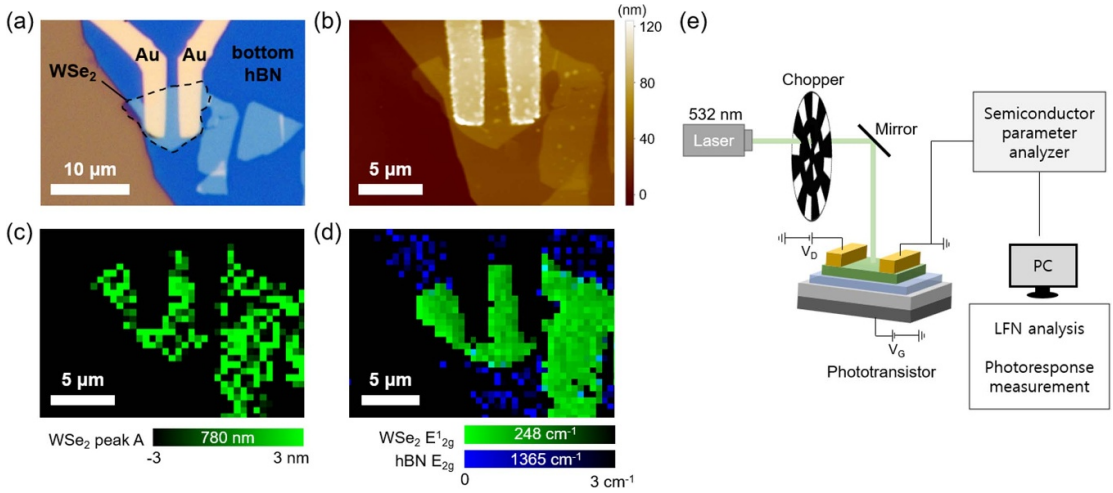

Figure 1. (a) The optical image, (b) the AFM image, (c) the PL mapping image, and (d) the Raman mapping image of the WSe_2/hBN device. (e) The schematic of the phototransistor experimental setup.

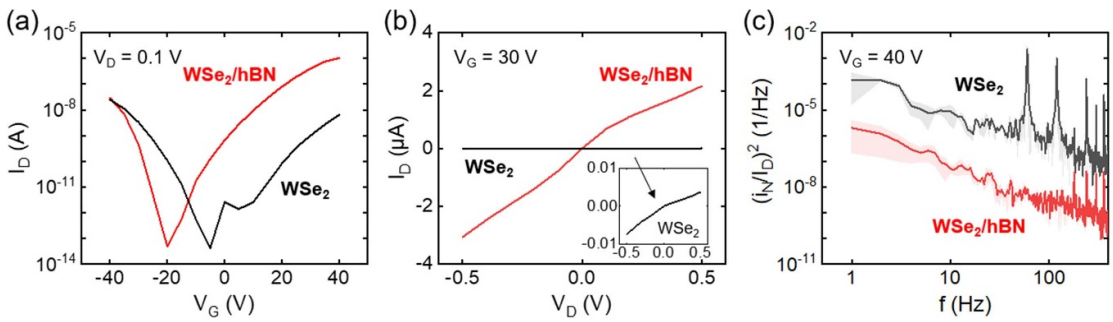

Figure 2. (a) The transfer characteristics for the WSe_2 and WSe_2/hBN devices at $V_D = 0.1$ V. (b) The output characteristics for the WSe_2 and WSe_2/hBN devices at $V_G = 30$ V. (c) The normalized noise of the WSe_2 and WSe_2/hBN devices at $V_G = 40$ V.

supplementary information. The LFN was 100 times lower in the WSe_2/hBN device than in the WSe_2 device, which shows that hBN can effectively suppress the LFN. Additionally, LFN reduction was consistent across various gate voltages (figure S6 of the supplementary information). Note that contact configuration was consistently maintained as gold-top contacts for all devices, so it is reasonable to attribute the observed reduction in LFN to the hBN passivation effect.

The enhanced electron transport and reduced LFN can be attributed to the passivation effect of hBN, which mitigates the impact of defects such as oxygen dangling bonds and surface charge traps typically present on SiO_2 dielectrics. Oxygen dangling bonds are known to act as p-type dopants in the WSe_2 channel, while surface charge traps contribute to increased LFN and decreased carrier transport properties [14, 16]. Introducing an hBN passivation layer thus leads to improved electrical performance and LFN suppression.

Figure 3(a) shows that the WSe_2 and the WSe_2/hBN devices exhibited clear photoresponse. In addition, the current of the WSe_2/hBN device was much more stable than that of WSe_2 alone, indicating that the WSe_2/hBN device generated less LFN. Likewise, in other devices, WSe_2/hBN devices consistently demonstrated lower current fluctuations (supplementary figure S7). Both devices exhibited very fast photoresponse of a few milliseconds, but the WSe_2/hBN device showed quicker response time (supplementary figure S8). The more comparisons of optoelectronic performances between the WSe_2 and WSe_2/hBN devices are shown in figures 3(b) and (c). Figure 3(b) plots the responsivity ($R = I_{ph}/P_{eff}$, where I_{ph} is the photocurrent and P_{eff} is the effective incident power to the channel), which is the power-to-photocurrent conversion ratio [19, 20]. As shown in figure 3(b), it can be observed that regardless of the power of the laser, the responsivity of the WSe_2/hBN device was always 100 times higher than that of the WSe_2 device. Figure 3(c) further solidifies the WSe_2/hBN device's superior optoelectronic properties by plotting the specific detectivity ($D^* = R\sqrt{AB}/i_N$, where A is the area of the device, B is the bandwidth, and i_N is the noise current), which is the sensitivity of the device [19, 20]. We calculated the specific detectivities based on the $1/f$ noise using LFN analysis for an accurate evaluation. Note that if we consider shot noise to be

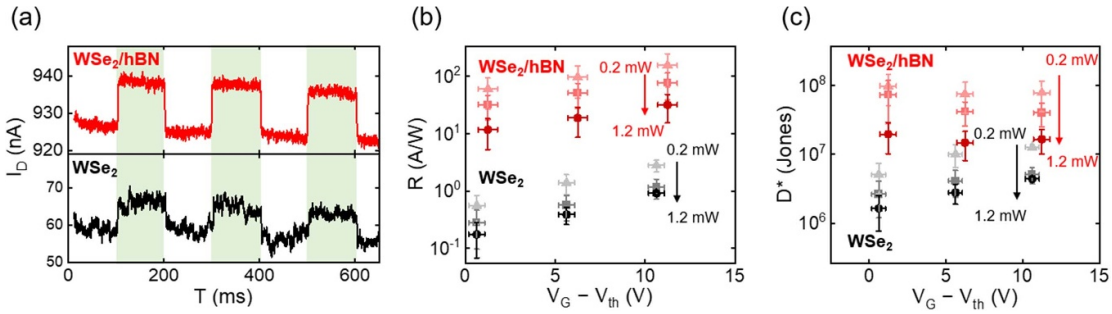

Figure 3. (a) The phototresponses, (b) the responsivity, and (c) the specific detectivity of the WSe_2 and WSe_2/hBN devices.

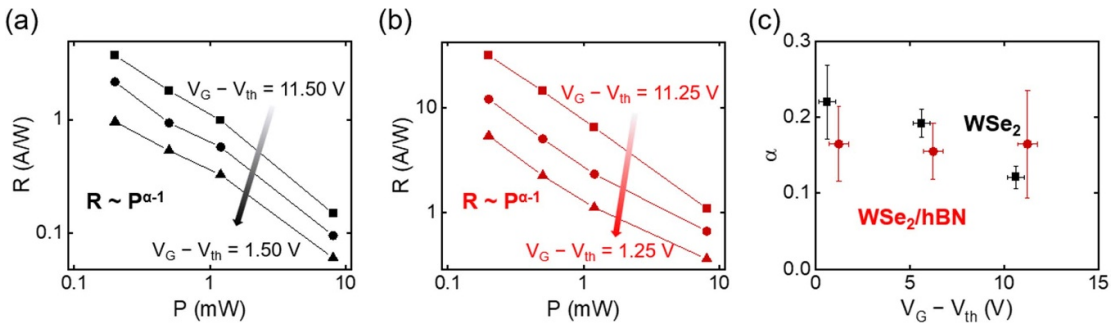

Figure 4. The responsivity of (a) the WSe_2 and (b) WSe_2/hBN devices fitted to a power law for incident power. (c) The gate voltage dependence of the α.

the only primary noise source, the specific detectivity is overstated (supplementary figure S9) [18]. The WSe_2/hBN device displayed a 10-fold improvement in specific detectivity over the WSe_2 device due to its lower LFN and higher responsivity.

The photogating effect is a plausible contributor to enhanced photodetection performance. As one of the primary photogeneration mechanisms in 2D TMDs, the photogating effect has been well known to enhance photocurrent and photodetection performance through channel gating [35–37]. Its influence can be evaluated based on the power-law relationship between responsivity and incident power ($R \sim P^{\alpha-1}$), where a smaller value of α in the expression indicates a dominant photogating contribution. The α value reflects the degree of the photogating effect under different gate voltages. Figures 4(a) and (b) present the responsivity of the WSe_2 and WSe_2/hBN devices, fitted using the power-law relation to extract α values. As shown in figure 4(c), the contribution of the photogating effect was nearly identical in both types of devices. This suggests that applying the hBN layer had minimal impact on the photogeneration mechanisms and that the improvement in photodetection performance was attributed to other factors, like reduced Coulomb scattering and suppressed defects.

Figure 5 illustrates the mechanisms of how hBN enhances photodetection performance. The amorphous nature of SiO_2 results in a high density of surface defects, leading to a poorly defined interface upon integration with WSe_2, characterized by numerous oxygen dangling bonds and surface charge traps that can trap electrons from the neighboring channel and introduce electrical noise (figure 5(a)) [38]. In contrast, hBN forms a clean interface with WSe_2 through van der Waals interaction and physically separates them from the underlying SiO_2 [39, 40]. Using a passivation layer effectively reduces the WSe_2 channel from Coulomb scattering induced by surface charges on SiO_2, thereby improving electron transport (figure 5(b)). When the light is illuminated on the WSe_2/hBN device, the photogenerated carriers can flow more efficiently, resulting in enhanced photocurrent. Additionally, the effect of surface traps and Coulomb scattering is minimized, leading to reduced LFN. As a result, the suppression of LFN and increased photocurrent directly translated into enhanced photodetection performance. The improvement is attributed to the passivation provided by hBN; therefore, the enhancement can be universally observed under laser illumination conditions that excite carriers in WSe_2.

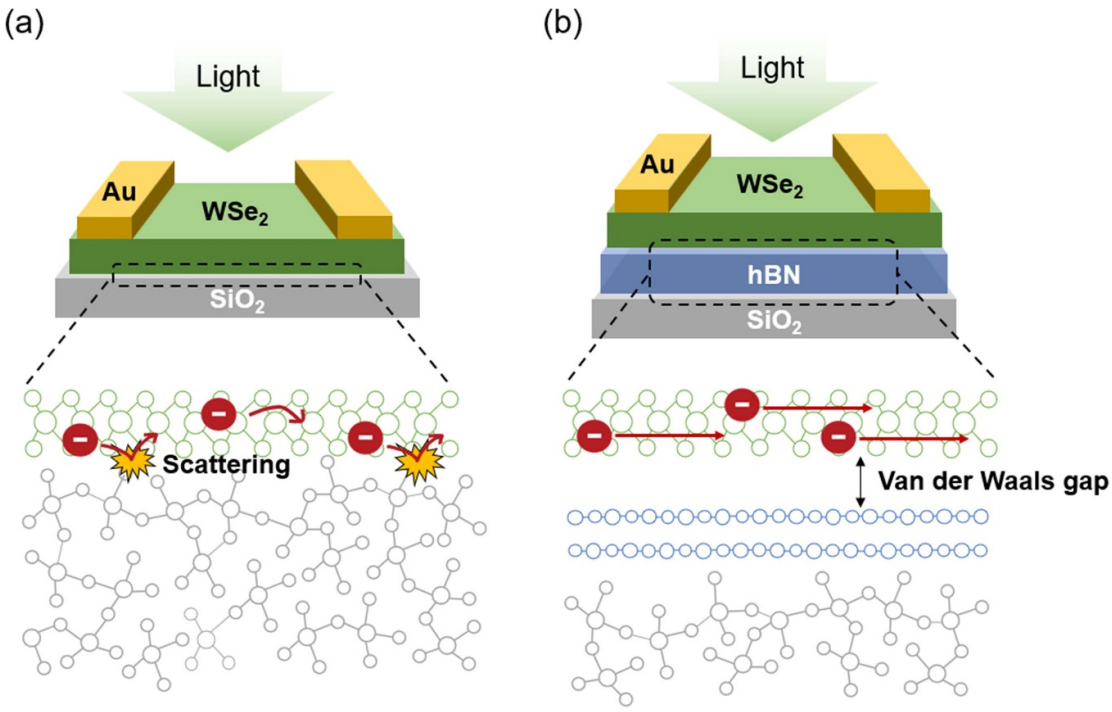

Figure 5. The schematics about the electron transport properties of (a) the WSe_2 and (b) the WSe_2/hBN devices.

4. Conclusion

In this study, we demonstrated that passivating the scattering sites of SiO_2 dielectric using hBN effectively suppresses dielectric disorder and enhances the photodetection performance of WSe_2 phototransistors. Optoelectrical and LFN analysis showed that our WSe_2/hBN devices exhibited near a 100-fold enhancement in responsivity and LFN reduction and a 10-fold increase in specific detectivity compared to pristine WSe_2 devices. These improvements are attributed to forming a clean van der Waals interface, which minimizes interfacial charge scattering and preserves the intrinsic electronic properties of the WSe_2 channel. These findings underscore the critical role of dielectric engineering in 2D optoelectronic devices and highlight dangling-bond-free materials as effective passivation materials for suppressing interfacial disorder and enhancing the performance of optoelectronic devices.

Data availability statement

All data that support the findings of this study are included within the article (and any supplementary files).

Acknowledgments

The authors appreciate the financial support of the National Research Foundation of Korea (NRF) Grant (Nos. 2021R1A2C3004783, 2021R1C1C2091728, and RS-2023-00220471) and the Nano Material Technology Development Program Grant (No. 2021M3H4A1A02049651) through NRF funded by the Ministry of Science and ICT (MSIT) of Korea.

ORCID iDs

Taehee Kim 0009-0007-2653-2282
Takhee Lee 0000-0001-5988-5219

References

[1] Chhowalla M, Jena D and Zhang H 2016 Two-dimensional semiconductors for transistors *Nat. Rev. Mater.* **1** 16052
[2] Jena D 2013 Tunneling transistors based on graphene and 2-D crystals *Proc. IEEE* **101** 1585–602
[3] Kim I, Higashitarumizu N, Rahman I K M R, Wang S, Kim H M, Geng J, Prabhakar R R, Ager J W and Javey A 2024 Low contact resistance WSe_2 p-Type transistors with highly stable, CMOS-compatible dopants *Nano Lett.* **24** 13528–33

[4] Tsai D-S, Liu K-K, Lien D-H, Tsai M-L, Kang C-F, Lin C-A, Li L-J and He J-H 2013 Few-layer MoS_2 with high broadband photogain and fast optical switching for use in harsh environments *ACS Nano* **7** 3905–11
[5] Huang L *et al* 2022 Enhanced light–matter interaction in two-dimensional transition metal dichalcogenides *Rep. Prog. Phys.* **85** 046401
[6] Wurstbauer U, Miller B, Parzinger E and Holleitner A W 2017 Light–matter interaction in transition metal dichalcogenides and their heterostructures *J. Phys. D: Appl. Phys.* **50** 173001
[7] Hu Z, Wu Z, Han C, He J, Ni Z and Chen W 2018 Two-dimensional transition metal dichalcogenides: interface and defect engineering *Chem. Soc. Rev.* **47** 3100–28
[8] Ahmed S and Yi J 2017 Two-dimensional transition metal dichalcogenides and their charge carrier mobilities in field-effect transistors *Nanomicro Lett.* **9** 50
[9] Wang G, Chernikov A, Glazov M M, Heinz T F, Marie X, Amand T and Urbaszek B 2018 Colloquium: excitons in atomically thin transition metal dichalcogenides *Rev. Mod. Phys.* **90** 021001
[10] Chen X, Lian Z, Meng Y, Ma L and Shi S-F 2023 Excitonic complexes in two-dimensional transition metal dichalcogenides *Nat. Commun.* **14** 8233
[11] Kang J, Tongay S, Zhou J, Li J and Wu J 2013 Band offsets and heterostructures of two-dimensional semiconductors *Appl. Phys. Lett.* **102** 012111
[12] Choi J-M, Jang H Y, Kim A R, Kwon J-D, Cho B, Park M H and Kim Y 2021 Ultra-flexible and rollable 2D-MoS_2/Si heterojunction-based near-infrared photodetector via direct synthesis *Nanoscale* **13** 672–80
[13] Miyamoto Y, Yoshikawa D, Takei K, Arie T and Akita S 2018 Effect of buffer layer on photoresponse of MoS_2 phototransistor *Jpn. J. Appl. Phys.* **57** 06HB01
[14] Raja A *et al* 2019 Dielectric disorder in two-dimensional materials *Nat. Nanotechnol.* **14** 832–7
[15] Jena D and Konar A 2007 Enhancement of carrier mobility in semiconductor nanostructures by dielectric engineering *Phys. Rev. Lett.* **98** 136805
[16] Dolui K, Rungger I and Sanvito S 2013 Origin of the n-Type and p-Type conductivity of MoS_2 monolayers on a SiO_2 substrate *Phys. Rev. B* **87** 165402
[17] Lee G-H *et al* 2013 Flexible and transparent MoS_2 field-effect transistors on hexagonal boron Nitride-Graphene heterostructures *ACS Nano* **7** 7931–6
[18] Ryoo S *et al* 2025 Noise-reduced WSe_2 phototransistors for enhanced photodetection performance via suppression of metal-induced gap states *Adv. Mater. Technol.* **10** 2500064
[19] Long M, Wang P, Fang H and Hu W 2019 Progress, challenges, and opportunities for 2D material based photodetectors *Adv. Funct. Mater.* **29** 1803807
[20] Jiang J, Wen Y, Wang H, Yin L, Cheng R, Liu C, Feng L and He J 2021 Recent advances in 2D materials for photodetectors *Adv. Electron. Mater.* **7** 2001125
[21] Yu Z *et al* 2016 Realization of room-temperature phonon-limited carrier transport in monolayer MoS_2 by dielectric and carrier screening *Adv. Mater.* **28** 547–52
[22] Cui Y *et al* 2015 High-performance monolayer WS_2 field-effect transistors on high-κ dielectrics *Adv. Mater.* **27** 5230–4
[23] Cheng C H and Chin A 2014 Low-voltage steep turn-on pMOSFET using ferroelectric high-κ gate dielectric *IEEE Electron Device Lett.* **35** 274–6
[24] Si M *et al* 2018 Steep-slope hysteresis-free negative capacitance MoS_2 transistors *Nat. Nanotechnol.* **13** 24–28
[25] Ma N and Jena D 2014 Charge scattering and mobility in atomically thin semiconductors *Phys. Rev. X* **4** 011043
[26] Shokouh S H H, Jeon P J, Pezeshki A, Choi K, Lee H S, Kim J S, Park E Y and Im S 2015 High-performance, air-stable, top-gate, p-channel WSe_2 field-effect transistor with fluoropolymer buffer layer *Adv. Funct. Mater.* **25** 7208–14
[27] Wang X *et al* 2015 Ultrasensitive and broadband MoS_2 photodetector driven by ferroelectrics *Adv. Mater.* **27** 6575–81
[28] Dean C R *et al* 2010 Boron nitride substrates for high-quality graphene electronics *Nat. Nanotechnol.* **5** 722–6
[29] Fukamachi S, Solís-Fernández P, Kawahara K, Tanaka D, Otake T, Lin Y-C, Suenaga K and Ago H 2023 Large-area synthesis and transfer of multilayer hexagonal boron nitride for enhanced graphene device arrays *Nat. Electron.* **6** 126–36
[30] Zeng H *et al* 2013 Optical signature of symmetry variations and spin-valley coupling in atomically thin tungsten dichalcogenides *Sci. Rep.* **3** 1–5
[31] Iwański J *et al* 2024 Revealing polytypism in 2D boron nitride with UV photoluminescence *npj 2D Mater. Appl.* **8** 1–9
[32] Cuscó R, Gil B, Cassabois G and Artús L 2016 Temperature dependence of Raman-active phonons and anharmonic interactions in layered hexagonal BN *Phys. Rev. B* **94** 155435
[33] Wang F, Zhang T, Xie R, Wang Z and Hu W 2023 How to characterize figures of merit of two-dimensional photodetectors *Nat. Commun.* **14** 2224
[34] Rogalski A 2022 Detectivities of WS_2/HfS_2 heterojunctions *Nat. Nanotechnol.* **17** 217–9
[35] Island J O, Blanter S I, Buscema M, Van Der Zant H S J and Castellanos-Gomez A 2015 Gate controlled photocurrent generation mechanisms in high-gain In_2Se_3 phototransistors *Nano Lett.* **15** 7853–8
[36] Sim J *et al* 2024 Enhanced photodetection performance of an *in situ* core/shell perovskite-MoS_2 phototransistor *ACS Nano* **18** 16905–13
[37] Fang H and Hu W 2017 Photogating in low dimensional photodetectors *Adv. Sci.* **4** 1700323
[38] Illarionov Y Y *et al* 2019 Ultrathin calcium fluoride insulators for two-dimensional field-effect transistors *Nat. Electron.* **2** 230–5
[39] Ali F, Choi H, Ali N, Hassan Y, Ngo T D, Ahmed F, Park W-K, Sun Z and Yoo W J 2024 Achieving near-ideal subthreshold swing in p-Type WSe_2 field-effect transistors *Adv. Electron. Mater.* **10** 2400071
[40] Fang N, Toyoda S, Taniguchi T, Watanabe K and Nagashio K 2019 Full energy spectra of interface state densities for n- and p-Type MoS_2 field-effect transistors *Adv. Funct. Mater.* **29** 1904465